Design of a CMG for underwater robots

Conference Paper · July 2011

DOI: 10.1109/Oceans-Spain.2011.6003401 · Source: IEEE Xplore

CITATIONS
3

READS
275

4 authors, including:

Eugenio Yime
University of Atlántico
58 PUBLICATIONS **307** CITATIONS
SEE PROFILE

Hector Moreno Avalos
Autonomous University of Coahuila
41 PUBLICATIONS **219** CITATIONS
SEE PROFILE

Roque J. Saltaren
Universidad Politécnica de Madrid
180 PUBLICATIONS **1,765** CITATIONS
SEE PROFILE

Design of a CMG for Underwater Robots

Eugenio Yime
Department of Mechanical and Mechatronics Engineering
Universidad Tecnológica de Bolívar
Campus Tecnológico de Ternera
Cartagena de Indias - Colombia
eyime@unitecnologica.edu.co

Héctor Moreno, Roque Saltarén and Rafael Aracil
Center for Automation and Robotics
Technical University of Madrid-CSIC
Calle José Gutierrez Abascal, 2.
28006. Madrid. Spain
{hmoreno, rsaltaren, aracil}@etsii.upm.es

***Abstract*— In this paper we present a Control Moment Gyroscope (CMG) for underwater robots. This is a single gimbal CMG with pyramid type configuration. This device has a modular design and is self-contained (i.e., all mechanical and electrical parts are contained in the CMG's hull.) The mechanical, electrical and electronic components of the CMG are described, and two experimental test are carry out to demonstrate the system functionality.**

I. Introduction

Control Moment Gyroscopes (CMGs) are angular momentum exchange devices used as torque actuators in spacecrafts and submarines, [1], [2]. According to Kurokawa, CMGs are classified by the number of gimbals, and are known as: single gimbal CMGs (SGCMGs) or double gimbal CMGs (DGCMGs). SGCMGs are studied actively because of their advantages of torque amplification and mechanical simplicity when compared to DGCMGs. Both types of CMGs have singularity problems as a disadvantage; this problem is more severe in SGCMGs [3].

Another classification is in terms of the configuration of the gyroscopes. The configuration is defined by the set of principal axes of each gyroscope. In the case of SGCMGs the principal axes are the gimbal axes. Configurations of SGCMGs are: pyramid type, skew type, symmetric type and multiple type. The most studied is the pyramid type, because it has the smallest number of gyroscopes, only four, having a minimum redundancy compared to a three dimensional couple. This redundancy allows to perform internal readjustments without producing an effective torque, this kind of motion is called null motion.

In this paper we present the design of a pyramid type SGCMG intended to be used in Underwater Robots. We describe the main characteristics of this CMG and explain its functionality. This paper is distributed as follows: in the following section the mechanical, electrical and electronic components of the CMG are described. In section III the workspace and capabilities of the CGM are discussed. In section IV two experimental tests and results are presented, and finally the conclusions in section V.

II. Design of the CMG

Fig. 1 shows the CAD design of the CMG. This is a pyramid type SGCMG with a redundancy of one degree. This redundancy allows internal readjustments of flywheels directions without producing an effective torque. This is called a null motion, a useful characteristic for evading internal singularities. In the following subsections, the mechanical, electrical and electronic components are described in more detail.

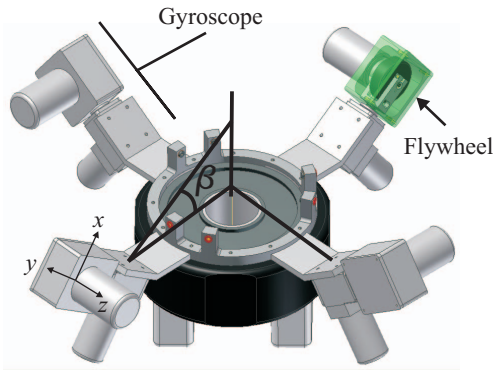

Fig. 1. CAD Design of the CMG

A. Mechanical Components

The materials used to build the CMG are stainless steel, aluminum and PVC. Stainless steel is used in thin or small parts where high strength is required, for example the actuator shafts. Also the flywheel is made of stainless steel to provide a greater moment of inertia. Aluminum is used in the gyroscope bases and the engine covers to reduce weight without losing strength. In addition, aluminum allows dissipation of heat generated by the electronics and motors. The hull of the CMG is made of PVC, due to its low weight and sealing. The purpose of the hull is to protect electronic components from water, and to dissipate the heat generated by electronics, which is accomplished through an aluminium plate.

B. Electrical Components

Each gyroscope is actuated by two electric motors, the flywheel motor and the gimbal motor. The flywheel motor is a 25 $watts$ Maxon Motor ECMax22. This actuator is directly coupled to the flywheel and is required to accelerate the inertia up to 10000 rpm. The gimbal motor is a 16 $watts$

978-1-61284-4577-0088-0/11/$26.00 ©2011 IEEE

Maxon Motor ECMax16, coupled with a planetary gearbox of $231:1$ reduction. The maximum velocity of the gimbal is $10\ rpm$.

C. Electronic Components

1) Motor Controllers: A loop of four motion controllers Maxon DEC 24/1 are responsible for controlling the speed of the flywheels. Each DEC has three inputs: one digital input for setting the motor direction of rotation; another digital signal for enabling / disabling the amplifier power stage; and one analog signal in the range of 0 to 5 V for setting the desired motor speed. The output of the DEC is a pulse-width modulated, PWM, proportional to the speed of the motor. This output is converted back to voltage with an external circuit, so it will be a controller card input.

The gimbal motors are controlled with four Maxon EPOS 24/1 motor controller which are in velocity mode of operation. Each EPOS 24/1 are commanded throught a CAN network, using the CANopen communication protocol. The CANopen master is the controller card, and the four EPOS are the slaves. The advantages of using a CAN network are, less complexity by using only three wires to communicate all devices, and a great speed of communication that goes up to 1 Mbps. Additionally, in the gimbal motor it was necessary to use digital inputs for detecting the CMG home position. The home position is when the total angular momentum is zero.

2) Inertial Measurement Unit: The inertial unit, IMU, is the Microstrain $3DM-GX1$, which allows a rotation of 360 degrees in the three axes. Communication is performed by $RS-232$. This IMU is able to capture, at the same time, the orientation in quaternion format, the angular velocity and the Earth's magnetic field vector. The maximum operating speed is $100\ Hz$, i.e. an interval of $10\ ms$ at each data collection.

3) Controller Card: The controller card is an embedded system based on PC104. It is responsible for commanding the motion of the gimbal motors, and read the data from the inertial measurement unit. A PC104 CAN card is employed to carry out the CAN communication with the EPOS 24/1. The PC104 card uses an analog output to command the speed of the gyroscopes flywheels through DEC 24/1 drivers. A RS-232 port is used for communication with the inertial unit. The ethernet port is used for communication with the main computer, situated in the underwater robot or in the base.

III. Modeling and Workspace

The workspace of the CMG is defined by all possible angular momentum vectors that can be achieved when rotating gimbal axes. Fig. 2 illustrates a CMG with pyramidal shape, the angle β is the pyramid skew angle, and θ_i are the gimbals angles for each i^{th}-axis, where $i = (1, .., 4)$. The mass and the inertia of each flywheel are represented by m_i and $\mathbf{I}_i$, respectively.

The angular momentum of one flywheel is $\mathbf{h}_i = \mathbf{I}_i\dot{\theta}_i\mathbf{z}_i$, where $\dot{\theta}_i$ is the time derivative of θ_i and $\mathbf{z}_i$ is the axes of the flywheel.

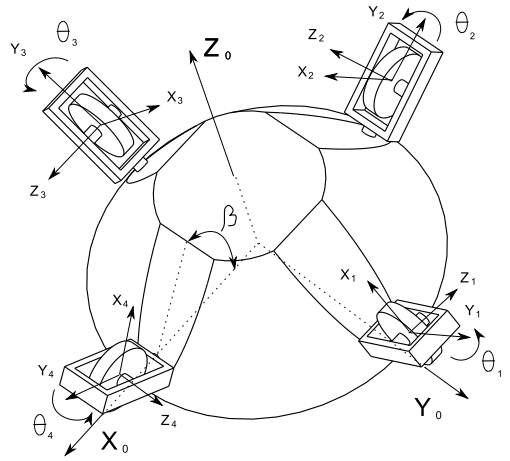

Fig. 2. CMG scheme

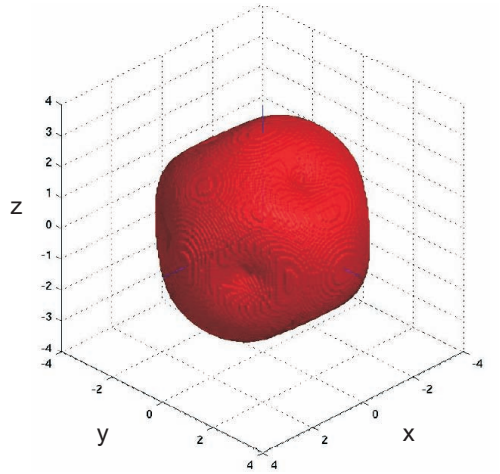

Fig. 3. Workspace of the CMG

If all flywheels have the same angular momentum, $h_0 = I\dot{\theta}$, then the total angular momentum is,

$$\mathbf{h}_t = h_0(\mathbf{z}_1 + \mathbf{z}_2 + \mathbf{z}_3 + \mathbf{z}_4) \tag{1}$$

A. Workspace

The CMG workspace is obtained by an iterative procedure in which the value of angle θ_i for each gimbal axis change between $-\pi \leq \theta_i \leq \pi$. Fig. 3 plots the results for $\mathbf{h}_t/h_0$, see (1). The workspace is the total angular momentum of the gyroscope, therefore what matters when the CMG is used as a torque exchange device is the offset within that graph and not a specific point. For example, if the system starts from rest, the origin of the system illustrated in the figure, and reaches the end of the workspace at any point, the average torque during the movement is $\tau_p = (\mathbf{h}_f - \mathbf{h}_i)/\Delta t = \mathbf{h}_f/\Delta t$. Besides, if the system is at a point in the surface of the workspace, $\|\mathbf{h}_f\|$ is maximal, and it can not produce torque in directions pointing away from the workspace.

On the other hand, if the system is near the boundary of the workspace, it can produce torque in either direction, but

the magnitude is limited in certain directions because a very large torque would be outside the workspace.

The torque, produced by a motion in the gimbal motors, is obtained from the derivative of the angular momentum:

$$\tau_t = \dot{\mathbf{h}}_t = h_0(\dot{\mathbf{z}}_1 + \dot{\mathbf{z}}_2 + \dot{\mathbf{z}}_3 + \dot{\mathbf{z}}_4) \tag{2}$$

where $\dot{\mathbf{z}}_i = \dot{\theta}_i \mathbf{x}_i$. This equation can be written in the following way:

$$\tau_t = h_0 \mathbf{X} \dot{\Theta} \tag{3}$$

where $\dot{\Theta} = \begin{bmatrix} \dot{\theta}_1 & \dot{\theta}_2 & \dot{\theta}_3 & \dot{\theta}_4 \end{bmatrix}^T$ is the vector of gimbal velocities, and the matrix

$$\mathbf{X} = \begin{bmatrix} \mathbf{x}_1 & \mathbf{x}_2 & \mathbf{x}_3 & \mathbf{x}_4 \end{bmatrix} \tag{4}$$

where:

$$\mathbf{x}_1 = \begin{bmatrix} s\theta_1 & -c\beta c\theta_1 & s\beta c\theta_1 \end{bmatrix}^T$$
$$\mathbf{x}_2 = \begin{bmatrix} c\beta c\theta_2 & s\theta_2 & s\beta c\theta_2 \end{bmatrix}^T$$
$$\mathbf{x}_3 = \begin{bmatrix} -s\theta_3 & c\beta c\theta_3 & s\beta c\theta_3 \end{bmatrix}^T$$
$$\mathbf{x}_4 = \begin{bmatrix} -c\beta c\theta_4 & s\theta_4 & s\beta c\theta_4 \end{bmatrix}^T$$

If the speed of the axes of the gimbals, $\dot{\Theta}$, lies in the nullspace of the matrix $\mathbf{X}$, there is not any movement. If the system is at a singular state, then there is not possible to generate a motion in a certain direction. The unit vector that defines the null motion in a pyramid type CMG, is:

$$\dot{\Theta}_{null} = \begin{bmatrix} \mathbf{x}_2^T \tilde{\mathbf{x}}_3 \mathbf{x}_4 \\ \mathbf{x}_3^T \tilde{\mathbf{x}}_4 \mathbf{x}_1 \\ \mathbf{x}_3^T \tilde{\mathbf{x}}_1 \mathbf{x}_2 \\ \mathbf{x}_1^T \tilde{\mathbf{x}}_2 \mathbf{x}_3 \end{bmatrix} \tag{5}$$

Equation (3) can be used to study the singularities of the CMG. Singularities occur when the determinant of $\mathbf{X}\mathbf{X}^T$ is zero. When the system is in a singular state the Jacobian rank decreases to a value lower than three, making impossible for the CMG to produce a torque in some directions, which are known as *singular directions*. The first work to study singularities in SGCMGs was performed by Margulies and Aubrun [4], other important studies were conducted by Bedrossian et al.[1], Kurokawa[5] and Bong Wie[6].

Fig. 4 is obtained using the algorithm presented in [7] to generate the workspace. Two types of singularities are shown: the external singularities, located on the limit of the workspace; and internal singularities within the workspace. Internal singularities are classified in elliptic and hyperbolic singularities. The elliptic singularity is a case of critical singularity in which the system can not escape using only the null motion. On the other hand, an hyperbolic singularity can be avoided by using null motion.

B. Dynamics

If $\mathbf{I}_i^i$ is the flywheel inertia expressed in its local frame, and $\mathbf{I}_0$ is the inertia of base body; then the total inertia for the system, $\mathbf{I}_t$, is,

$$\mathbf{I}_t = \mathbf{I}_0 + \sum_{i=1}^{4} (\mathbf{R}_i \mathbf{I}_i^i \mathbf{R}_i^T - m_i \tilde{\mathbf{r}}_i \tilde{\mathbf{r}}_i) \tag{6}$$
$$= \mathbf{I}_0 + \mathbf{D} \tag{7}$$

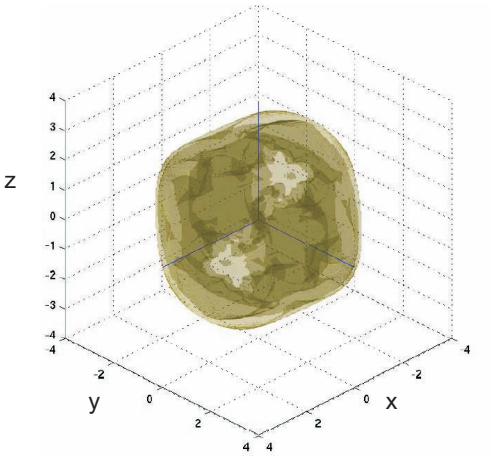

Fig. 4. Singularities of the CMG

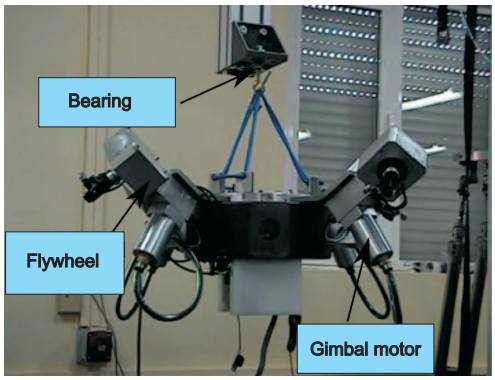

Fig. 5. First test

Where $\mathbf{r}_i$ is the position of i^{th}-flywheel. Therefore, the dynamic equation of the overall system is,

$$\boldsymbol{\tau}_{ext} = \mathbf{I}_t \dot{\boldsymbol{\omega}}_0 + \tilde{\boldsymbol{\omega}}_0 \mathbf{I}_t \boldsymbol{\omega}_0 + \boldsymbol{\tau}_{gyro} \tag{8}$$
$$\boldsymbol{\tau}_{ext} = \mathbf{I}_0 \dot{\boldsymbol{\omega}}_0 + \mathbf{D} \dot{\boldsymbol{\omega}}_0 + \tilde{\boldsymbol{\omega}}_0 \mathbf{I}_t \boldsymbol{\omega}_0 + \boldsymbol{\tau}_{gyro} \tag{9}$$

Where $\boldsymbol{\tau}_{gyro}$ is the required torque by the control law, and it is produced by the steering law through the motion of gimbals axis. Symbols $\boldsymbol{\omega}_0$, $\dot{\boldsymbol{\omega}}_0$ are used to represent the angular velocity vector and the angular acceleration vector of the base body, respectively.

IV. Experimental

Two experimental tests were planned to verify the functionality of the gyroscopes. The CMG is controlled by means of the control strategy that we introduced in [8]. The goal of the first test is to verify the performance of the control algorithm for a required change of rotation of the body. Fig. 5 illustrates the prototype prior to the test. The CMG is supported by a rotational joint which allow rotations around a vertical axis.

The rotations were made about the z axis of the CMG. The movements were: 40 degrees counterclockwise, 80 degrees clockwise to -40 degrees, 100 degrees counterclockwise up

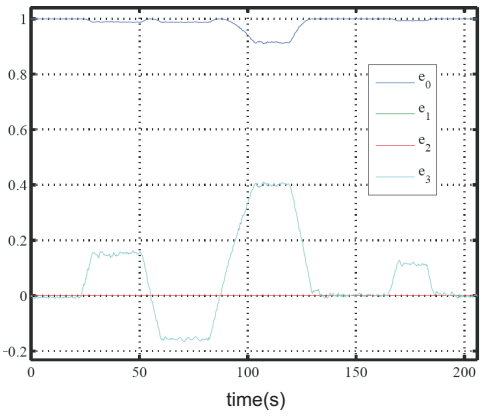

Fig. 6. Orientation of the CMG

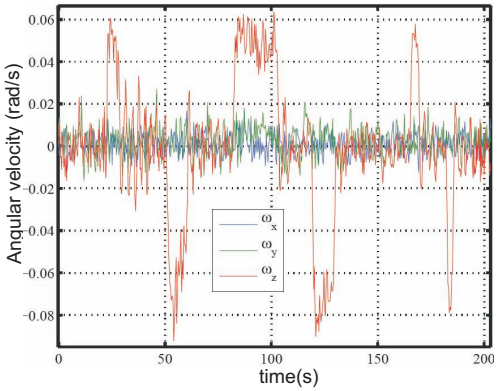

Fig. 7. Angular velocity

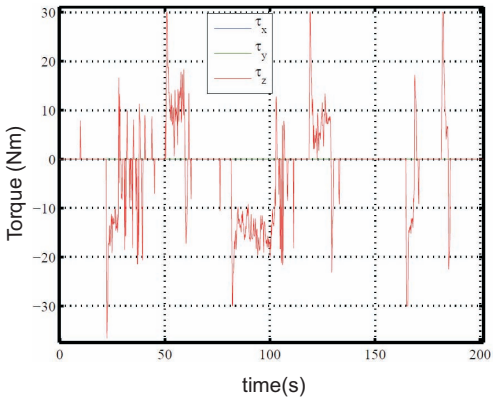

Fig. 8. Control law

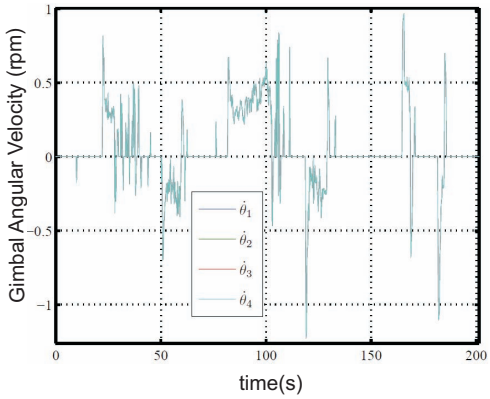

Fig. 9. Steering law

to 60 degrees, 60 degrees counterclockwise up to 0, and finally a 20 degrees turn and return to zero.

Figures 6 and 7 show the values of the body orientation expressed in quaternion form, and the angular velocity. The orientation values are given with respect to the starting position of the system. The first change begins around 20 sec, the second starts at 50 sec, between 150 and 160 sec, the body has returned to its original position before rotating 20 degrees.

To reduce the effect of the noise on the IMU signal to the controller, we analyzed the results when the IMU is static, it was observed that the magnitude of the noise is 0.02 rad/s, so if the norm of the velocity is in this range the controller considers that the body is at rest. In the case of quaternions, the norm of the noise is 0.01. For control purposes it is considered that the body has reached the desired goal if the norm of the quaternion error between desired and actual quaternion is less than or equal to this value. Figures 8 and 9 show the values returned by the controller and steering law. Both signals have signal noise due to the IMU. A fact to highlight in the figure of velocities is that for rotations around the z axis the velocity of the four gyroscopes is the same. The peaks that appear when system is static, are due to the noise of the signals, since the system is near to the desired goal.

Fig. 10 shows the position of the gimbal motor in degrees. The values are obtained from the encoder of each motor. there are intermittent movements in the first and third task, this is due to a small imbalance in the test equipment that makes the system rotate clockwise because of the effects of gravity. The net effect is that the gyros do not return to zero when the body returns to its initial position in the second task.

The second test consisted in perturbing the system in the initial position. Fig. 11 shows the prototype prior to the test. As can be seen the external pair occurs along the direction [-1, 1, 0], allowing to verify the response in the x and y axes. Once the perturbation stops, the controller must return the body to its original position.

The results of orientation and angular velocity of the second experiment are shown in Figures 12 and 13. The first disturbance occurs at 4 sec, the system is stabilized around the 10 sec, then a second disturbance occurs at 13 sec, making the system oscillate. The controller is able to stabilize the system around the 45 sec. The oscillations occur due to the flexibility introduced by the mechanical fasteners of the test model.

Figures 14 and 15 show the response of the controller and steering law for the second case. The first peak occurs during

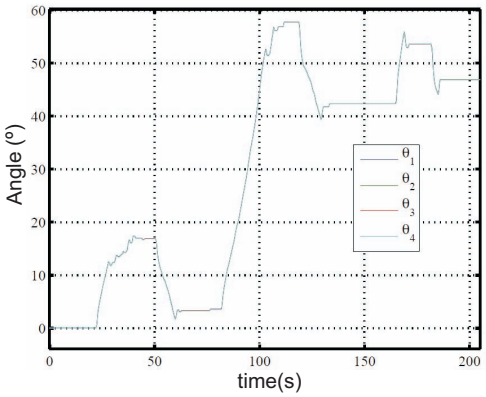

Fig. 10. Angles of the gimbals

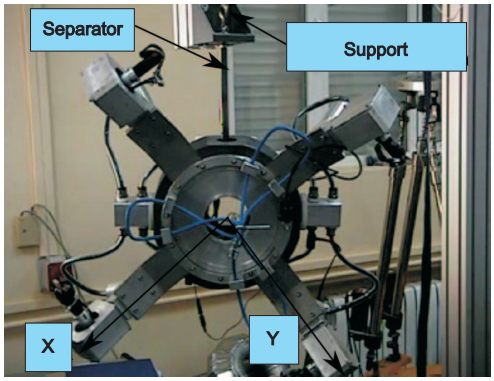

Fig. 11. Second test

the perturbation and begins to decline as the system begins to move toward the starting point. Around the 7 sec, the angular velocity reaches its maximum, at this point the controller torque has fallen to almost zero and subsequently grows (in negative sense) to slow down the body as it approaches the target. In 10 sec the body has returned to its starting point and both the controller torque and steering law velocities are zero.

In the case of the second perturbation, vibration is introduced by the disturbance and flexibility in the fasteners, and it makes the driver continue to send signals up to the 44 sec, when the body stops moving. In the first disturbance the system quickly stabilizes and in the 10 sec the gimbal motors remains constant.

V. Conclusions

In this paper the design a CMG, was presented. This is a single gimbal CMG with pyramid type configuration. It was designed in a modular way for easy assembly and disassembly with an underwater robot. The CMG was controlled using a sliding mode controller for improving system robustness to uncertainties and unknown dynamics. We presented the results of two experimental test that were carry out in order to verify the control law and the system functionality. First test were made with several rotations around z axis. The results showed a well behaved system. Second test showed

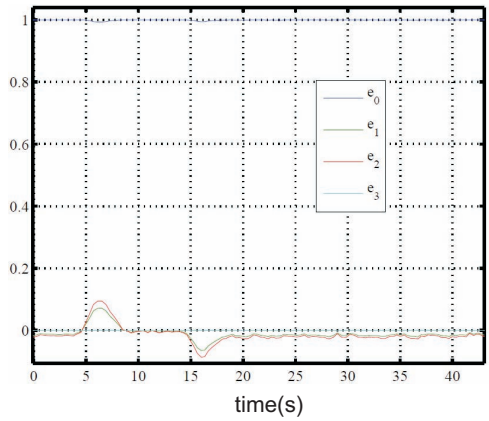

Fig. 12. Orientation

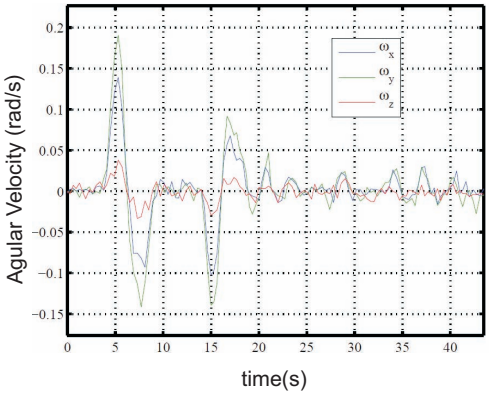

Fig. 13. Angular velocity

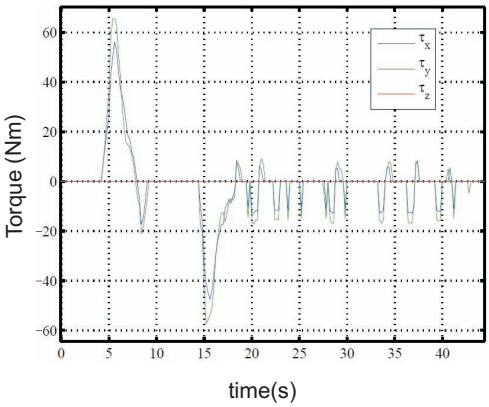

Fig. 14. Control law

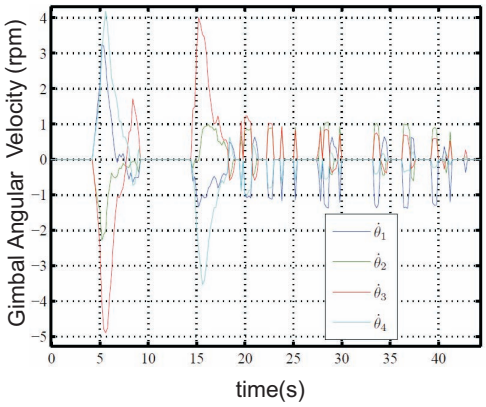

Fig. 15. Steering law

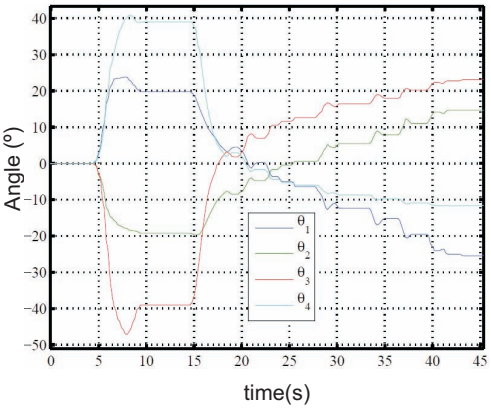

Fig. 16. Angles of the gimbals

a fast controller capable of dealing with external disturbance while keeping the system in a desired orientation.

VI. Acknowledgement

This work is supported by the project DPI2006-06493 of the Spanish Science and Education Ministery.

References

[1] N. S. Bedrossian, J. Paradiso, E. V. Bergmann, and D. Rowell, "Redundant single gimbal control moment gyroscope singularity analysis," *J. Guidance*, vol. 13, no. 6, pp. 1096–1101, 1990.

[2] B. Thornton, T. Ura, Y. Nose, and S. Turnock, "Internal actuation of underwater robots using control moment gyros," *IEEE Oceans 2005*, vol. 1, pp. 591–598, 2005.

[3] H. S. Oh and S. R. Vadali, "Feedback control and steering laws for spacecraft using single gimbal control moment gyros," *J. Astronautical Sciences*, vol. 39, no. 2, pp. 183–203, 1991.

[4] G. Margulies and J. N. Aubrun, "Geometric theory of single-gimbal control moment gyro systems," *Journal of the Astronautical Sciences*, vol. 26, no. 2, pp. 159–191, 1978.

[5] H. Kurokawa, "A geometric study of single gimbal control moment gyros, singularity problems and steering law," Intelligent Systems Institute, National Institute of Advanced Science and Technology, 1-2-1 Namiki, Tsukuba, Ibaraki 305-8564 Japan, Tech. Rep. 175, 1988.

[6] B. Wie, "Singularity analysis and visualization for single-gimbal control moment gyro systems," *Journal of Guidance, Control and Dynamics*, vol. 27, no. 2, pp. 271–282, 2004.

[7] R. Saltaren, R. Aracil, C. Alvarez, E. Yime, and J. Sabater, "Field and service applications - exploring deep sea by teleoperated robot - an underwater parallel robot with high navigation capabilities," *Robotics Automation Magazine, IEEE*, vol. 14, no. 3, pp. 65–75, sep. 2007.

[8] E. Yime, J. Quintero, R. Saltaren, and R. Aracil, "A new approach to avoid internal singularities in cmg with pyramidal shape using sliding control," in *IFAC European Control Conference, ECC 09*, 2009.